Determination of Orientational Order in Deformed Glassy PMMA from Solid-State NMR Data

Michael Wendlandt,[†] Jacco D. van Beek,[‡] Ulrich W. Suter,[†] and Beat H. Meier*,[‡]

Department of Materials, ETH Zurich, 8093 Zürich, Switzerland, and Physical Chemistry, ETH Zurich, 8093 Zürich, Switzerland

Received June 9, 2005; Revised Manuscript Received July 27, 2005

ABSTRACT: The orientational distribution function for polymer chain segments in plain-strain compressed glassy poly(methyl methacrylate) is evaluated, as a function of two polar angles, from a series of one-dimensional deuterium NMR spectra. The experimental data are analyzed using a tailored regulatory approach. For low degrees of orientational order, the choice of the regularization scheme is shown to become critical and two-dimensional Tikhonov−Phillips regularization yielded the best results for the present study.

I. Introduction

Determination and modeling of the development of the spatial orientation of chain segments with deformation in polymer solids has been a subject of discussion in numerous publications.[1−14] Experimental methods that characterize orientational distributions include X-ray scattering,[4−7] birefringence,[8,9] and solid-state nuclear magnetic resonance (NMR) spectroscopy.[1−3,9−14] The advantage of solid-state NMR, as a means to measure orientation, is that the structural units (labeled segments along a polymer chain), of which the orientation is measured, are well-defined. Moreover, the method is not restricted to certain moments of the orientational distribution like in the case of birefringence measurements. However, for the extraction of structural information from NMR spectra, one is faced with solving a so-called *ill-posed inverse problem*: even though the calculation of a spectrum from an orientational distribution function (ODF) is trivial, this is no guarantee for finding a stable and unique solution when extracting the ODF from the noisy experimental spectrum. Strategies to treat such problems, i.e., *regularization*, are well established in several fields of science[15−18] and have been applied to solid-state NMR before to determine ODFs as a function of one[19−28] or two structural parameters[29−34] from one-dimensional or multidimensional NMR spectra.

Here we describe a method for determining low degrees of orientational order of deuterium-labeled chain segments in a polymer which has been deformed plastically in the glassy state. The experimental data obtained from poly(methyl methacrylate) (PMMA) consist of a series of static one-dimensional (1D) deuterium (^{2}H) spectra, each for a different orientation of the sample with respect to the magnetic field B_0. Such data are easy to obtain and are, therefore, an interesting alternative to the two-dimensional (2D) DECODER experiment,[12,35−38] which has been used to address similar problems.

The main focus of this paper is to develop a reliable method for monitoring the orientation of individual segments of the polymer chains in a glassy polymer as a function of plastic deformation. A detailed investigation on the molecular interpretation of strain-induced order in PMMA, based on the methods discussed here, is presented in a subsequent publication.[39]

II. Experiments and Data-Evaluation Schemes

Theoretical descriptions of the mechanical deformation behavior of glassy polymers can be found in references 40−42. In the study discussed here, plane-strain compression[39] was used, which results in a high reproducibility of stress−strain behavior. In contrast to tensile deformation, which can be classified as a strongly aligning mode of deformation,[43] compressive deformation is only weakly aligning and results in lower degrees of orientational order of the chain segments. Investigation of such weakly oriented systems presents an experimental challenge, however.

A. Reconstruction of Orientational Distributions of Chain-Segments from Solid-State NMR Spectra. An Inverse Ill-Posed Problem. A detailed description of inverse methods in NMR spectral analysis with two-dimensional parameter spaces has been published elsewhere.[14] In all but the simplest situations, the inverse problem can only be solved if additional constraints or assumptions are used in the analysis. If one does not want to resort to using specific models for the distributions to be evaluated, regularization methods are commonly applied. Such methods allow for an efficient implementation of smoothness constraints for the resulting distribution; e.g., simple and smooth parameter distributions become favored over complex oscillatory distributions. This additional "common sense" constraint leads then to a unique solution of the ill-posed problem. In the following, a brief summary of the theoretical background will be presented to point out the novel aspects of the analysis applied here.

We define a discrete (NMR)spectrum $s(\omega)$ which is governed by the local orientational polar angles θ and ϕ. The spectrum is a superposition of n contributions from chain segments oriented at (θ_i,ϕ_i), weighted by their statistical weight $g(\theta,\phi)$ and mapped onto m frequency points ω_j through the linear matrix operator $K(\omega,\theta,\phi)$, i.e.

$$s(\omega) = K(\omega,\theta,\phi)\, g(\theta,\phi) \tag{1}$$

[†] Department of Materials, ETH Zurich.
[‡] Physical Chemistry, ETH Zurich.

10.1021/ma0512105 CCC: $30.25 © 2005 American Chemical Society
Published on Web 09/01/2005

where $s(\omega)$ and $g(\theta,\phi)$ are vectors of dimensions n and m, respectively, and $K(\omega,\theta)$ is an $m \times n$ matrix ($m > n$), the columns of which correspond to the "basis" spectra $[s_1^0, s_2^0, ..., s_n^0]$ that reflect the spectrum for a given set of parameters (θ_i,ϕ_i). It is the aim to extract the distribution $g(\theta,\phi)$ from the experimental spectrum $s(\omega)$ with the help of complete knowledge of the direct problem, i.e., the kernel $K(\omega,\theta,\phi)$, by inversion of the mapping of eq 1, which for continuous variables corresponds to a Fredholm integral equation of the first kind.[44] It is well-known that such integrals are *ill-posed* in the sense of Hadamard;[45] i.e., existence, uniqueness, and stability of solutions cannot be taken for granted.

Generally speaking, the existence criterion is always violated in experimental data analysis since experimental noise is not implemented in $K(\omega,\theta,\phi)$. Hence an obvious choice for the inverse solution of eq 1 is a least-squares (LS) fit that minimizes the discrepancy between the measured and a simulated spectrum according to

$$\min||K(\omega,\theta,\phi)g(\theta,\phi) - s(\omega)||^2 = ||K(\omega,\theta,\phi)\tilde{g}(\theta,\phi) - s(\omega)||^2 \quad (2)$$

where $||\vec{x}|| = \sqrt{\sum_i x(i)\cdot x(i)}$ and $\tilde{g}(\theta,\phi)$ is a reasonable approximation to the true solution $g(\theta,\phi)$ capturing experimental noise. A solution to the discrete LS problem of eq 2 can be found, for example, by singular value decomposition (SVD)[46] of the Kernel K

$$K = UWV^T \quad (3)$$

where U is an $m \times n$ sized column-orthogonal matrix, W an $n \times n$ sized diagonal matrix with the singular values w_l as its elements, and V an $n \times n$ sized orthonormal matrix. The solution $\tilde{g}(\theta,\phi)$ of the LS problem is given by

$$\tilde{g}(\theta,\phi) = \sum_{l=1}^{n} \frac{1}{w_l} v_l(u_l^T \cdot s) \quad (4)$$

with n the number of basis spectra in the kernel K, and u_l, v_l columns of U and V. Uniqueness is violated by the coexistence of several solutions $\tilde{g}(\theta,\phi)_i$ ($\tilde{g}(\theta,\phi)_x \neq \tilde{g}(\theta,\phi)_y$ if $x \neq y$), with equivalent misfits for a given noisy spectrum $s(\omega)$. Violation of stability is reflected by the fact that close proximity in the spectral data space of two spectra $s_1(\omega)$ and $s_2(\omega)$ does not necessarily result in close proximity of the corresponding generating functions $\tilde{g}_1(\theta,\phi)$ and $\tilde{g}_2(\theta,\phi)$.

Restoring Stability by Regularization. To restore stability to the inverse problem, one needs to introduce additional information and thus additional restrictions on $\tilde{g}(\theta,\phi)$, e.g., by mapping the degree of violation of a restriction onto a scalar number $R[\tilde{g}(\theta,\phi)]$. The regularized LS problem is given by

$$||K(\omega,\theta,\phi)\tilde{g}(\theta,\phi) - s(\omega)||^2 + \lambda_{reg} R[\tilde{g}(\theta,\phi)] \rightarrow \min! \quad (5)$$

Here λ_{reg} is the so-called regularization parameter, which balances between the quality of the fit in the spectral domain and the impact of the additional restriction.

A rather general regularization approach is to ask for a "smooth" solution $\tilde{g}(\theta,\phi)$ assuming that the probability distribution $g(\theta,\phi)$ generally does not change abruptly with a small variation of $g(\theta,\phi)$. Tikhonov regularization[47−49] is a commonly-used approach to implement smoothness by asking for a small quadratic norm of $(\tilde{g}(\theta,\phi) - \tilde{g}_0(\theta,\phi))$ leading to a regularization term

$$R_{Tik}[\tilde{g}(\theta,\phi)] = ||\tilde{g}(\theta,\phi) - \tilde{g}_0(\theta,\phi)||^2 \quad (6)$$

where $\tilde{g}_0(\theta,\phi)$ is an optional rough estimate of the expected solution such that the fit is biased toward $\tilde{g}_0(\theta,\phi)$. In the literature the estimate $\tilde{g}_0(\theta,\phi)$ is often chosen to be zero, such that the minimization is biased toward the solution with the smallest norm. In this case, i.e., $\tilde{g}_0(\theta,\phi) = 0$, the solution of eq 5 is

$$\tilde{g}(\theta,\phi) = \sum_{l=1}^{n} \frac{w_l}{w_l^2 + \lambda_{reg}} v_l(u_l^T \cdot s) \quad (7)$$

i.e., the $1/w_l$ dependence of eq 4 has become $w_l/(w_l^2 + \lambda_{reg})$, which means a reduction of the disturbing effects of the high-order singular values. A different way to imply smoothness in *one-parameter problems* is to ask for a small quadratic norm of the second derivative of the solution, leading to the so-called Tikhonov−Philips regularization term[50]

$$R_{TP}[\tilde{g}(\theta)] = ||\tilde{g}_{\theta\theta}||^2 \quad (8)$$

where $\tilde{g}_{\theta\theta} = \partial^2\tilde{g}(\theta)/\partial\theta^2$. For distributions exhibiting sharp edges in combination with flat regions, more advanced edge-preserving smoothness constraints may be applied.[51] However, this study addresses *two-parameter problems*, i.e., ODFs need to be reconstructed as a function of two polar angles (θ,ϕ). The problem of finding a measure for the smoothness of a surface $S(x, y, z) = S(\theta,\phi,\tilde{g}(\theta,\phi))$ has been discussed in detail in the field of computational vision. Grimson et al.[52] suggested a "quadratic variation" regularization term, which performed well in the reconstruction of smooth surfaces:[51]

$$R_{QV}[\tilde{g}(\theta,\phi)] = ||\tilde{g}_{\theta\theta}||^2 + 2\,||\tilde{g}_{\theta\phi}||^2 + ||\tilde{g}_{\phi\phi}||^2 \quad (9)$$

where $\tilde{g}_{xy} = \partial^2\tilde{g}/(\partial x\partial y)$. Often there is very little difference in results between Tikhonov and QV regularization, but as will be shown below, for this particular experiment the situation was different and QV was clearly better at regularizing the problem.

Determination of the optimal degree of regularization, i.e., finding the optimal balance between the severity of the constraint and the discrepancy between fit and experimental spectrum by a proper choice of the regularization parameter λ_{reg}, is a crucial point. Visualization of the influence of the constraint can be achieved by plotting the discrepancy $||K(\omega, \theta,\phi)\tilde{g}(\theta,\phi) - s(\omega)||^2$ against the regularization term $R[\tilde{g}(\theta,\phi)]$. Plotted on a logarithmic scale, such a plot often exhibits the shape of the letter "L", hence the name L-plot.[46] A rough estimate for the optimal regularization parameter is selected from the L-plot where the corner of the "L" is found. Note that other criteria to find the optimal regularization parameter are available,[46,53] but will not be discussed here, since our experience showed, that the L-curve criterion worked satisfactory for the functionals used in this study.

B. Materials and Sample Preparation. ^{2}H-labeled PMMA, cf. Figure 1, was chosen as a model system for the study of orientation of chain segments in a deformed

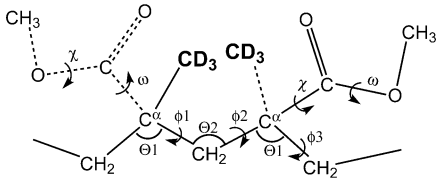

Figure 1. Chemical structure of a racemic dyad of ^{2}H labeled PMMA. Rotation angles of the backbone (ϕ_1, ϕ_2, ϕ_3, ...), and of the ester group (ω, χ) are shown as zero. As supported by energy calculations and WAXS data,[54,55] the most likely conformation is $\Theta_1 = 110°$, $\Theta_2 = 128°$, $\omega = \chi = 0°$, $\phi_1 = 10°$, $\phi_2 = 10°$, $\phi_3 = -10°$, $\phi_4 = -10°$. The ^{2}H-labeled α-methyl groups are emphasized in bold.

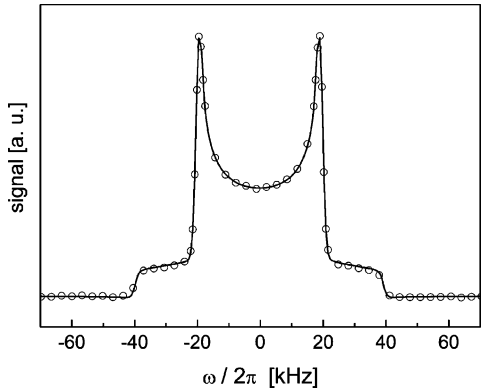

Figure 2. ^{2}H solid-state NMR spectrum of a non-deformed (isotropic) sample. Open circles: experiment ($S/N \approx 500$), solid line: simulation including rf-inhomogenity, using a quadrupole coupling constant $C_{qcc} = 52.7$ kHz.

polymer glass. All deuterated PMMA used for this study was obtained from Polymer Source Inc., Canada, with molecular weight $M_w = 75\,400$ and polydispersity of $M_w/M_n = 1.03$. The molecular structure of a racemic dyad is shown in Figure 1 where deuterium labeled methyl groups CD_3 are emphasized by bold letters. Plastic deformation of the glassy PMMA samples was achieved by plane-strain compression of rectangular samples, described in a sample fixed frame with z-axis along the direction of compression, y-axis along the direction of flow, and x-axis along the constant dimension of the sample.[39] Compression ratios $\lambda_z = l_z^{def}/l_z^0$ between 0.38 and 1 were employed.

C. The NMR Experiment. The information about orientational order contained in the NMR line shape is provided by the anisotropic nature of the quadrupole interaction. The α-methyl group rotation in PMMA at room temperature is fast compared to the NMR time scale[56−58] and the observed ^{2}H quadrupole tensor is axially symmetry with the unique axis along the three-fold axis of the methyl group (cf. Figure 1). Thus, in ^{2}H NMR, molecular order is monitored through the orientation of the unique axis of the methyl quadrupole tensor. Static 1D ^{2}H NMR spectra were obtained by a standard quadrupolar echo pulse: $90°_X-\tau-90°_Y-\tau-$acquire,[59] with $\tau = 31.2$ μs at an rf-field strength of 88.3 kHz. 1200 scans were coadded with a recycling delay of 0.7 s. Figure 2 shows the experimental spectrum of undeformed amorphous PMMA together with a simulated spectrum corresponding to an isotropic ODF. The simulated spectrum corresponds to a quadrupole coupling constant $C_{qcc} = 52.7$ kHz and was calculated using finite pulses and the non-negligible rf-inhomogeneity in the rf-coil, which was determined experimentally by a nutation spectrum, was accounted

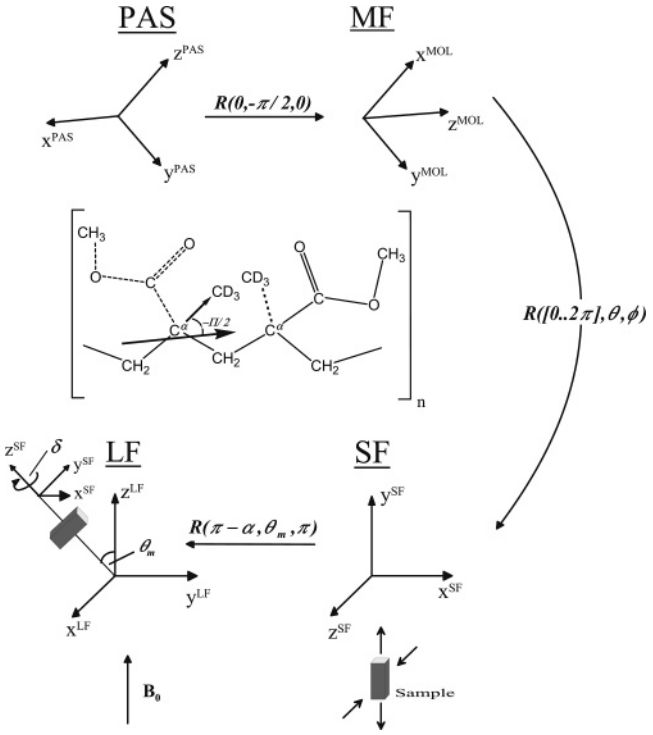

Figure 3. Right handed orthogonal frames used to describe the orientation of the principal axes system (PAS) relative to the laboratory frame (LF). The ODF of molecular segments is described by two angles (θ, ϕ), which rotate the molecular fixed frame (MF) into the sample fixed frame (SF). These angles are identical with the polar angles describing the orientation of the CH_2-CH_2 direction in the sample frame. The angle δ describes the stepwise rotation of the sample during the NMR experiment around an axis running perpendicular to the draw direction y^{SF} and tilted by the magic angle θ_m relative to Z^{LF}, where the case of $\delta = 0$ is defined with y^{SF} lying in the $z^{LF}-x^{LF}$ plane.

for in the simulation by superposition of a Gaussian part to the otherwise Lorentzian line-broadening in the time domain. This was found to be almost equivalent to taking into account the rf-distribution explicitly by calculating a weighted superposition of spectra with different rf-field strengths (not shown). To obtain the orientational distribution of molecular segments of the polymer chain relative to the unique directions of the deformation, it is convenient to introduce the following coordinate systems (see also Figure 3).

The *principal axes system* (**PAS**) of the CD_3 quadrupole tensor is oriented with z^{PAS} along the CD_3-C^α bond and x^{PAS} chosen to be colinear with the CH_2-CH_2 direction of the attached backbone carbons. We define a *molecular frame* (**MF**) such that z^{MOL} runs along the CH_2-CH_2 direction and x^{MOL} along the CD_3-C^α bond parallel to z^{PAS}. The transformation from the PAS to the molecular frame is, therefore, a simple 90° rotation. The *sample frame* (**SF**) is defined by the setup of the plane-strain compression experiment. Here x^{SF} is the dimension which is kept constant during deformation, y^{SF} is the dimension of elongation, and z^{SF} is the direction of compression. The transformation from molecular to sample frame contains the distribution of ϕ and ψ angles produced by the deformation. In the *laboratory frame* (**LF**) the z^{LF} describes the direction of the external magnetic field $\vec{B}_0$. The Euler rotations between frames are indicated in Figure 3 and follow the convention of ref 60. The angle δ is the angle that was increased stepwise to change the orientation of the

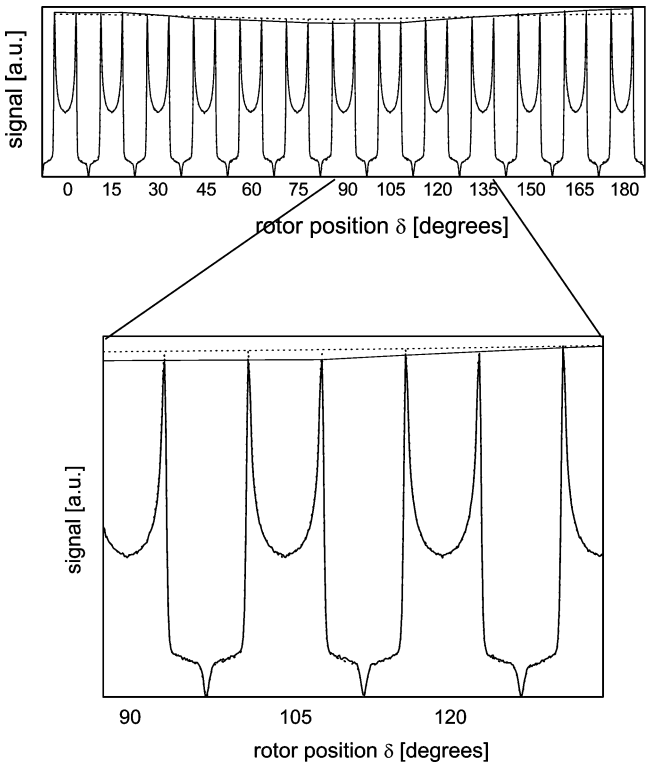

Figure 4. (Top) Serial plots of two series of a full cycle of 13 experimental 1D quadrupolar solid state NMR spectra of PMMA deformed (far) below the glass transition temperature with two different draw ratios. Each single spectrum corresponds to a different laboratory-frame-fixed orientation of the sample rotated stepwise with increments $\Delta\delta$ of 15° around an axis running perpendicular to the draw direction of the deformed sample. The values beneath each single 1D spectrum denote the actual sample position. Dotted line: PMMA compressed with $\lambda_z = l_z^{def}/l_z^0 = 0.53$ showing medium orientational order. Solid line: PMMA compressed with $\lambda_z = 0.42$ showing somewhat higher orientational order. For clarity, the envelope of each series is shown, indicating the different degrees of order. (Bottom) Magnification of the indicated range. All spectra were scaled to the same integral to eliminate intensity effects caused by minor changes in the resonance circuit upon repositioning of the sample.

sample towards the magnetic field within each series of 1D experiments belonging to a sample. The angles (θ, ϕ) give the information about the orientation of molecular segments relative to the SF. Note that the first angle in the transformation from MF to SF must be integrated over, as we assume that for each orientation of the molecular z-axis, described by θ and ϕ, an isotropic distribution of rotations of the MF around z^{MOL} will be present when averaged over the whole sample.

Thirteen spectra were obtained for each sample, with δ incremented in steps of $\Delta\delta = 15°$ around z^{SF}, which runs perpendicular to the flow direction y^{SF} of the deformed sample. Figure 4 shows serial plots of typical experimental series of 13 combined one-dimensional (1D) spectra obtained from two samples with different degrees of orientational order. These were deformed with compression ratios $\lambda_z = l_z^{def}/l_z^0 = 0.42$ and $\lambda_z = 0.53$, respectively. A completely isotropic sample would yield a serial plot of 13 identical 1D spectra. The deviation from an isotropic distribution can be illustrated by the envelope curves as shown in Figure 4 by the two solid lines connecting the maxima of the individual 1D spectra. Note that the number of 13 independent sample orientations was somewhat arbitrarily chosen. It was found to provide a reasonable balance between data acquisition time and information content. Up to a certain level, the information content can generally be increased by adding more independent spectra to the kernel but the measuring time increases linearly.

D. Analysis of the Experiment. Basis spectra of the Kernel K, which maps the ODF onto the NMR spectrum, were calculated using *GAMMA*[61] following a linear interpolation scheme for θ and ϕ, as described in ref 14 using the quadrupole coupling constant obtained from the fit of the non-oriented sample of Figure 2. Each interval $[[\theta_i, \theta_{i+1}], [\phi_j, \phi_{j+1}]]$ was integrated using a two-point Gaussian quadrature scheme with 3 intervals, leading to an effective resolution of approximately 1.8 degrees in each angle for the 10° grid resolution for the simulation used throughout the paper.

Solving of the arising ill-posed inverse problem was performed by regularization of the minimization problem, cf. eq 5, by a surface smoothness constraint as described in eq 9 together with the restriction of non-negativity for the ODF. Validation of this procedure will be discussed below, based on numerical testing. Minimization of the regularized functional was performed by a nonlinear minimization algorithm with non-negativity constraints[62] provided by Matlab, Version 6.5 R13, The MathWorks, Inc. A proper choice of the optimal regularization parameter was obtained graphically by the L-curve criterion.[46]

In literature, orientational distributions are often represented in terms of their moments, i.e. in terms of so-called "order parameters." Order parameters are connected with ODFs by the Wigner matrix elements (WMEs).[63] Every ODF can be expanded in terms of an infinite series of WMEs $\mathscr{D}^l_{mn}(\alpha,\beta,\gamma)$ since they represent a complete orthonormal basis[60,64]

$$P(\alpha,\beta,\gamma) = \sum_{l=0}^{l=\infty} \sum_{m=-l}^{m=l} \sum_{n=-l}^{n=l} c^l_{mn}\, \mathscr{D}^l_{mn}(\alpha,\beta,\gamma) \qquad (10)$$

where $P(\alpha,\beta,\gamma)$ is normalized as

$$\int_V P(\alpha,\beta,\gamma)\, \mathrm{d}V = 1 \qquad (11)$$

with $\mathrm{d}V = \sin\beta\ \mathrm{d}\beta\ \mathrm{d}\alpha\ \mathrm{d}\gamma$. The average Wigner matrix elements, or so-called *order parameters*, are defined as

$$\langle \mathscr{D}^l_{mn} \rangle = \int_V P(\alpha,\beta,\gamma) \mathscr{D}^l_{mn}(\alpha,\beta,\gamma)\, \mathrm{d}V \qquad (12)$$

These order parameters are related to the expansion coefficients c^l_{mn} of the Wigner expansion as

$$c^l_{mn} = \frac{2l+1}{8\pi^2} \langle \mathscr{D}^l_{mn} \rangle \qquad (13)$$

Symmetries of the orientational distribution function arising from the setup of the experiment or the sample preparation lead to constraints on the expansion coefficients.[42,65] In the present case, the symmetry of plane-strain compression of a polymer sample with initially isotropically distributed chain segments yields

$$P(\theta,\phi) = \sum_{l=0}^{l=\infty} \sum_{n=-l}^{n=l} c^l_{0n} \mathscr{D}^l_{0n}(0, -\theta, -\phi) \qquad (14)$$

where l and n are nonnegative even integer numbers.

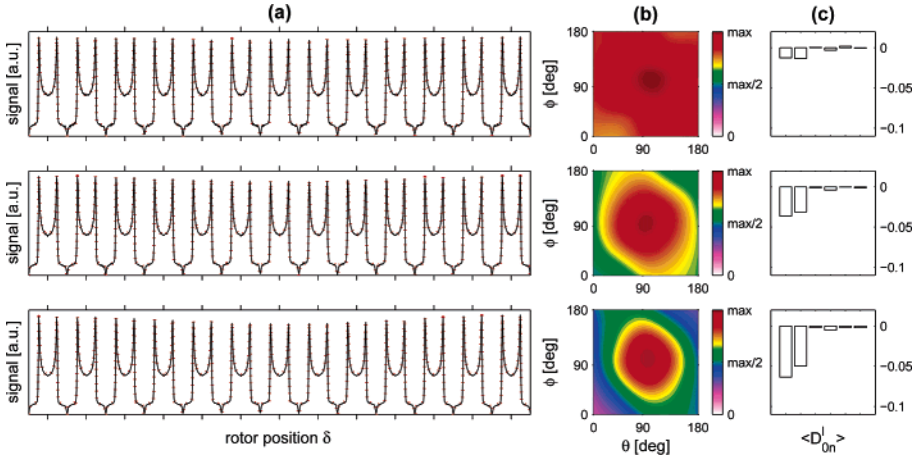

Figure 5. Reconstruction of ODFs from three representative experimental NMR spectra of deformed PMMA exhibiting different degrees of orientation corresponding-to-compression ratios of $\lambda_z = 0.835$, $\lambda_z = 0.764$, $\lambda_z = 0.636$ going from top to bottom. (a) experimental series of 13 1D spectra (black lines) with fits (red dots); (b) reconstructed ODFs using NN + quadratic variation for regularization of the spectral analysis; (c) expansion of (b) into order parameters showing $\langle \mathscr{D}^2_{00} \rangle$, $\langle \mathscr{D}^2_{02} \rangle$, $\langle \mathscr{D}^4_{00} \rangle$, $\langle \mathscr{D}^4_{02} \rangle$, $\langle \mathscr{D}^4_{04} \rangle$, and $\langle \mathscr{D}^6_{00} \rangle$.

The average WME with $l = 2$, $m = 0$, and $n = 0$, which is the most important coefficient for flat distributions, equals the average second Legendre polynomial or the so-called "Herman orientation parameter" $\langle \mathscr{D}^2_{00} \rangle = \langle P_2(\cos\theta) \rangle = \langle {}^1/_2(3\cos^2\theta - 1) \rangle$.[60]

III. Results and Discussion

Figure 5 shows three reconstructed ODFs of plastically deformed glassy PMMA with different compression ratios together with the experimental NMR spectra and order parameters from $\langle D^2_{00} \rangle$ to $\langle D^6_{00} \rangle$. Regularization was achieved using the QV-regularization term R_{QV} plus a restriction of the ODF to nonnegative (NN) values only. The sample deformation increases from top to bottom and correspondingly, the ODFs deviate more and more from an isotropic distribution. The ODFs reveal a maximum around ($\phi = \theta = 90°$), as expected from the plane-strain deformation setup, indicating that chain segments orient along the direction of flow. Expansion of the reconstructed ODFs in terms of order parameters are shown in Figure 5c.

To achieve an idea of the accuracy and reliability of the analysis, the response of the algorithm was tested using simulated data: In a first step, the spectrum of an nonoriented sample (cf. Figure 2) was fitted to ensure that no systematic spectral distortions, e.g., loss of intensity at the outer wings, are present. Such distortions would inevitably lead to strong artifacts in the analysis if not included in the simulation. In a second step, different *reasonable* input ODFs have been generated of which the corresponding NMR spectra have been calculated using eq 1. To classify the ODFs in terms of width of distribution as judged from the spectral domain, the squared deviation from an isotropic spectrum was used as a criterion:

$$\chi_s^2 = \frac{||(s_0 - s)||^2}{||s_0||^2} \tag{15}$$

where s_0 is the discrete NMR spectrum of an isotropic sample, and s is the discrete NMR spectrum of an oriented sample. After adding random noise to the spectra, the reconstructed output ODFs have been obtained using the regulatory analysis. The squared difference between the output and the input distribution, χ_g^2, was used as a numerical criterion for the power of the minimization algorithm:

$$\chi_g^2 = \frac{||ODF_{input} - ODF_{output}||^2}{||ODF_{input}||^2} \tag{16}$$

A crucial point is to find *reasonable* input ODFs which allow the comparison of simulated and experimental data. At this point, additional information (not contained in the NMR spectra) is used in the evaluation process: the reasonable ODFs are chosen according to their ability to faithfully represent a set of input ODFs that are thought to be typical for the distribution occurring in the experimentally deformed glassy polymer sample in this study. This assumption, as severe as it is, is still significantly less stringent than assuming a model function for the expected distribution. In the present study, plane-strain compression as the mode of deformation suggest that chain segments most probably orient along the direction of elongation, hence exhibiting a single peak at polar angles ($\phi = \theta = 90°$) within the sample fixed frame described in Figure 3. Furthermore, there are strong indications that certain structural units in polymer glasses, e.g. stiff chain segment, orient under plastic deformation according either to the so-called affine[12,39] or to the pseudo-affine model.[9,39,40,66,67] Hence initial simulation tests were performed with different single-peaked input ODFs according to the affine and pseudo-affine model. Later, these tests were expanded to single-peaked and multipeaked ODFs of Gaussian and Lorentzian shape. In total 600 input ODFs have been generated with varying width and symmetry and the corresponding NMR spectra were simulated and noise was added to obtain signal-to-noise ratios in the range of $S/N = 10-1000$. Here only results obtained from simulated spectra with $S/N = 233$ are shown, which corresponds to the lowest S/N that was observed experimentally. Results from simulated spectra with different signal-to-noise within the range of $S/N = 10-1000$ were in line with the conclusions presented in this study and indicated a high reliability of the suggested analysis even at very low $S/N < 100$.[68]

Figures 6 and 7 visualize the power of different regularization approaches. Input ODFs were simulated

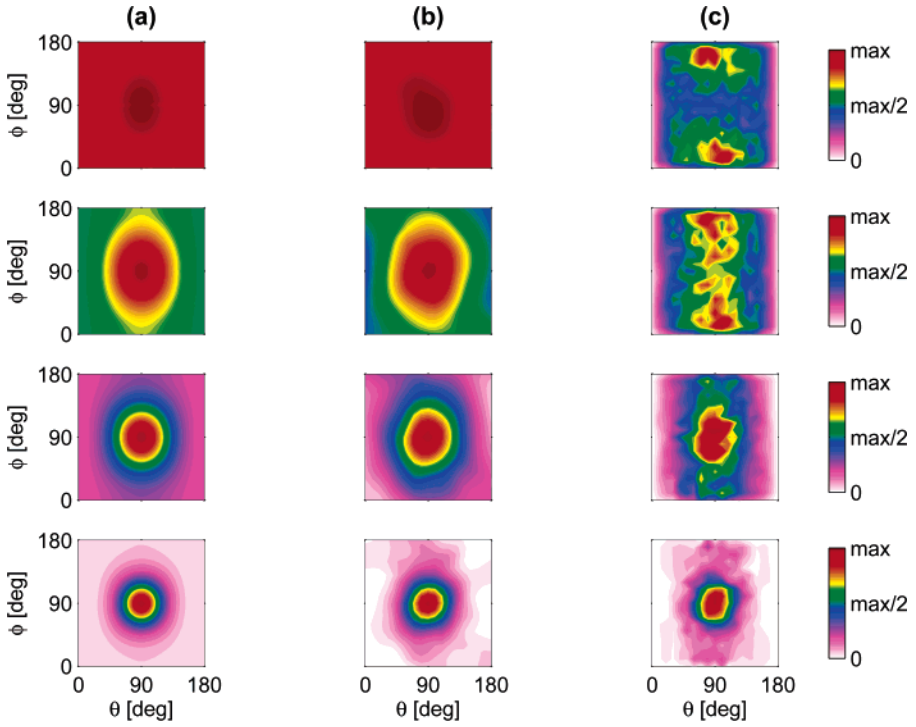

Figure 6. Visualization of the typical accuracy of the reconstruction of (a) ODFs that were calculated according to the affine model,[39] from simulated spectra with $S/N = 233$. Here the ODFs describe the distribution of stiff chain segments in a rubber-elastic network with an average of 3 stiff segments between two network points and compression ratios $\lambda_z = 0.92$, $\lambda_z = 0.64$, $\lambda_z = 0.36$, and $\lambda_z = 0.20$ going from top to bottom. The grid density was 10° in the parameter space. The simulated spectra correspond to values for χ_S of 0.0038, 0.0208, 0.0535, and 0.1041, going from least to most oriented. (b) Results obtained using NN + QV with relative errors $\chi_g = 0.017$, 0.038, 0.117, 0.114 going from top to bottom figure. (c) Results obtained for NN + Tikhonov regularization with $\tilde{g}_0(\theta,\phi) = 0$ with relative errors $\chi_g = 0.429$, $\chi_g = 0.372$, $\chi_g = 0.305$, and $\chi_g = 0.197$.

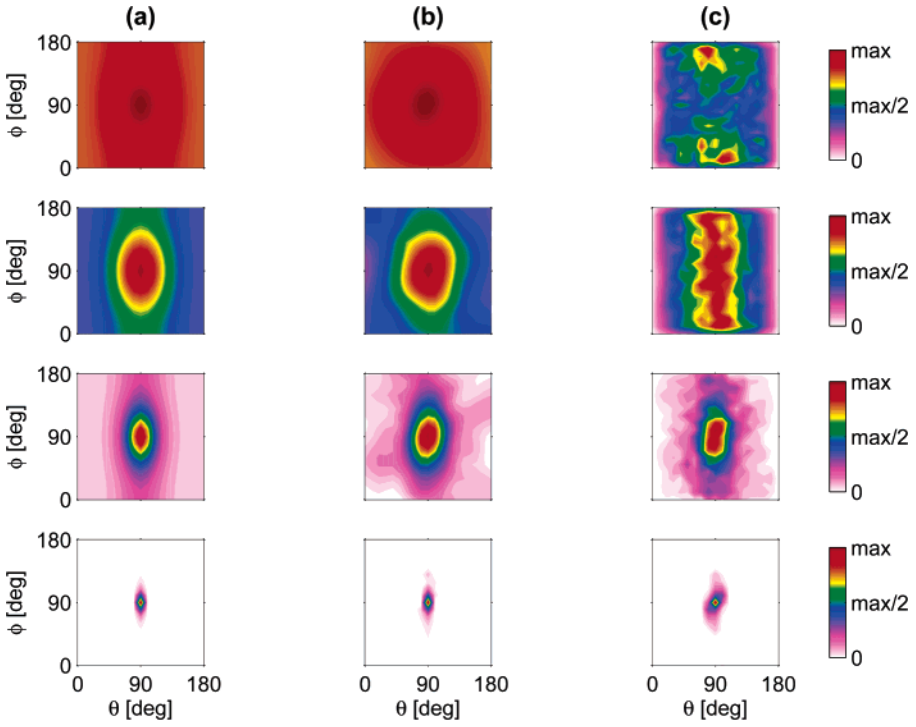

Figure 7. Visualization of the typical accuracy of the reconstruction of (a) ODFs that were calculated according to the pseudo-affine model, from simulated spectra with $S/N = 233$. Here the ODFs describe the distribution of independent orienting structural units for compression ratios $\lambda_z = 0.96$, $\lambda_z = 0.84$, $\lambda_z = 0.60$, and $\lambda_z = 0.20$. The grid density was 10 degrees in the parameter space. The simulated spectra correspond to values for χ_S of 0.0077, 0.0328, 0.0920 and 0.2103, going from least to most oriented. (b) Results obtained using NN + QV with relative errors $\chi_g = 0.029$, 0.066, 0.157, 0.211 going from top to bottom. (c) Results obtained for NN + Tikhonov regularization with $\tilde{g}_0(\theta,\phi) = 0$ with relative errors $\chi_g = 0.414$, $\chi_g = 0.315$, $\chi_g = 0.192$, and $\chi_g = 0.993$.

according to the affine model and the pseudo-affine model, respectively, with varying peak width and constant peak position at ($\phi = \theta = 90°$) for a grid resolution of 10° in the parameter space. It is striking to see that analysis employing the commonly used Tikhonov regularization leads for broad distributions to output ODF's

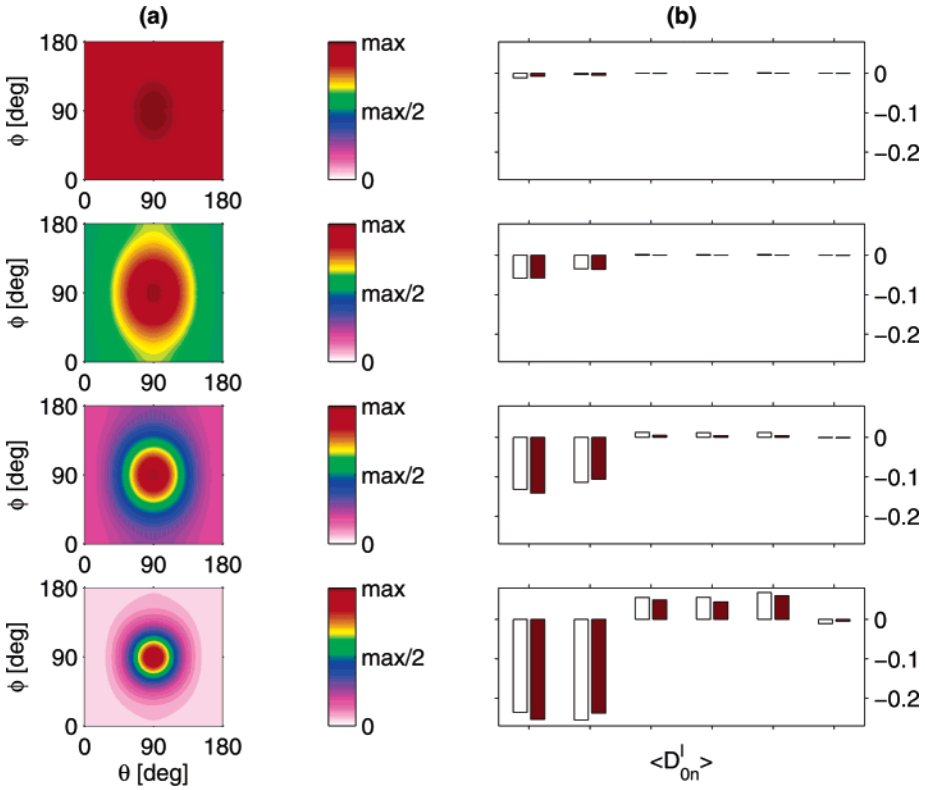

Figure 8. (a) Expansion into order parameters of the ODFs from the affine model. (b) Parameters $\langle\mathscr{D}^2_{00}\rangle$, $\langle\mathscr{D}^2_{02}\rangle$, $\langle\mathscr{D}^4_{00}\rangle$, $\langle\mathscr{D}^4_{02}\rangle$, $\langle\mathscr{D}^4_{04}\rangle$, and $\langle\mathscr{D}^6_{00}\rangle$ of input (white bars) and reconstructed (red bars) ODFs from simulated noisy spectra ($S/N = 233$) using NN + QV-regularization are shown.

that differ significantly from the input while QV reproduces the input rather faithfully. Note that the spectra corresponding to the Tikhonov and QV ODF's in Figures 6 and 7 are not distinguishable within *S/N* used. This behavior is a consequence of the weak dependence of the NMR spectra on variation of the angle ϕ. For more strongly peaked input ODFs, the resulting ODFs using QV and Tikhonov regularization became very similar. The same behavior was found for a number of other NMR experiments (not shown). The Tikhonov results of ref 33, for example, were fully reproduced with QV.

Further it was found that Gaussian ODFs with pronounced asymmetries could not be reconstructed satisfactorily with either regularization scheme.[68] However, this is not thought to be a drawback since experimental ODFs exhibiting such critical asymmetries are considered to have a negligible probability due to the plane-strain compression setup. Results obtained for simulated 2D DECODER experiments[68] indicate that 2D experiments would be more sensitive to the asymmetry of the Gaussian input ODFs. Nonetheless, anticipated artifacts in the corresponding 2D DECODER, e.g., mechanical instabilities, baseline distortions, spin diffusion, and lower *S/N*, were not included in the comparison. The QV smoothness constraint is, however, better suited to generate the "good" output ODF as found also for symmetric ODFs of Gaussian and Lorentzian shape.[68]

Moving from angle space to Wigner space, a different expression for the accuracy of the regulatory spectral analysis was obtained from the expansion of ODFs into order parameters $\langle\mathscr{D}^l_{mn}\rangle$. Relative errors of order parameters can be obtained in a similar way by expansion of the input and the reconstructed output distributions

Table 1. Maximum Relative Errors χ_g and $\chi_{\mathscr{D}^l_{mn}}$ between Order Parameters of Input and Reconstructed ODFs as Obtained from Simulated Data with Degrees of Orientation in the Experimentally Found Range of Spectra, $233 < S/N < 500$ and $0.013 < \chi_S < 0.036$[a]

	max. nonsymm	max symm.
χ_g	0.085	0.079
$\chi_{\mathscr{D}^2_{00}}$	0.130	0.075
$\chi_{\mathscr{D}^2_{02}}$	0.169	0.103
$\chi_{\mathscr{D}^4_{00}}$	1.9	0.215
$\chi_{\mathscr{D}^4_{02}}$	2.2	0.316
$\chi_{\mathscr{D}^4_{04}}$	1.9	0.93
$\chi_{\mathscr{D}^6_{00}}$	27.7	1.10

[a] ODFs were classified according to whether they were symmetric or nonsymmetric.

in terms of Wigner functions and calculation of the squared deviation $\chi^2_{\mathscr{D}^l_{mn}}$

$$\chi^2_{\mathscr{D}^l_{mn}} = \frac{||\langle\mathscr{D}^l_{mn}(input)\rangle - \langle\mathscr{D}^l_{mn}(output)\rangle||^2}{||\langle\mathscr{D}^l_{mn}(input)\rangle||^2} \quad (17)$$

Figure 8 presents the first six nonvanishing order parameters for the same input ODFs as shown in Figure 6 and reconstructed output ODFs. By compiling the deviations χ_g and $\chi^2_{\mathscr{D}^l_{mn}}$ for all the test distributions which are in the range of experimental conditions, i.e., $233 < S/N < 500$ and $0.013 < \chi_S < 0.036$, a measure for the accuracy of the analysis was achieved. The maximum values found for those ODFs are shown in Table 1 and are assumed to give a reliable approximation of the relative error corresponding to the current experimental ODFs. A division is made between symmetric and nonsymmetric ODFs to show the decrease in

accuracy with increased asymmetries in the input ODF. These results indicate that the algorithm is good at reconstructing symmetric ODFs and satisfactory for more asymmetric distributions such as those predicted by the affine and pseudo-affine model, for the near-isotropic distribution functions tested here. The high relative errors found for order parameters with $l \geq 4$ and higher are due to their small absolute numbers, which fall below the resolution of the NMR experiment in the present case of low orientational order. However, the values for $l \leq 2$ support the conclusion that QV-regularization is a powerful regularization scheme for this specific NMR experiment.

Other regularization approaches have also been tested but were found to suppress oscillations in the reconstructed ODFs, i.e., to overcome the ill-posedness of the inverse problem, less satisfactorily than QV.[68] These were either only NN or NN + Tikhonov with $\tilde{g}_0(\theta,\phi) = 1$. In some of the tested approaches the value for χ_g was in selected cases very high while the deviation in the order parameters could be as low as for QV. This indicates that those approaches are not able to stabilize the problem toward high-frequency oscillations but that this does not necessarily affect the lower order parameters.[68] Hence the reliability of the analysis increases if both, the ODF as a function of two polar angles, and their order parameters are considered complementary.

IV. Summary and Conclusions

A 1D solid-state NMR experiment was used to obtain information on spatial orientation of ^{2}H-labeled chain segments in glassy PMMA. The experiments consisted of a series of 13 1D quadrupolar echos, where each single spectrum corresponds to a static orientation of the glassy polymer sample with respect to the external magnetic field. Reconstruction of average orientational distribution functions (ODFs) of labeled chain segments as a function of two polar angles was achieved by a tailored regulatory analysis of the NMR spectra. The regularization implies a restriction of the reconstructed ODF to have a smooth nonnegative surface, where a numerical measure for the smoothness of the ODF was determined by the norm of its quadratic variation (QV). Simulation tests with different single-peaked input ODFs according to the so-called affine and pseudo-affine model, and additionally also single-peaked and multi-peaked ODFs of Gaussian and Lorentzian shape of varying peak widths and positions indicated that a satisfactory determination of the distribution function was possible using this approach. Nonetheless, the applied analysis does not give satisfactory results for ODFs with pronounced asymmetries since the NMR spectra were not sensitive enough toward this parameter variation. The application of QV-regularization in the analysis of simulated 2D DECODER spectra of the same critical asymmetric ODFs showed slightly better results. However, it cannot be concluded a priori that 2D DECODER experiments would yield better results in general, since anticipated typical artifacts in 2D experiments were not included in such a comparison.

Error estimates of experimental data, obtained from comparison with simulated ODFs, support the conclusion that the simple 1D quadropole-echo NMR experiment combined with the tailored regulatory spectral analysis represents a reliable and experimentally simple approach to quantify the orientational order of chain segments in glassy PMMA as a function of plastic deformation. A detailed analysis and discussion of orientation-strain relations of deformed linear and cross-linked PMMA, compressed above and below the glass transition temperature, will be discussed in a subsequent publication.[39]

A Matlab package "NLCSmoothReg" for the solution of ill-posed linear inverse problems for one and two-dimensional constraint solutions, according to the different regularization methods described in this study, is available free of charge via the Internet at http://www.mathworks.com/matlabcentral/fileexchange/.

Acknowledgment. This study has been supported in part by the Swiss National Science Foundation.

Supporting Information Available: Figures showing reconstruction of symmetric and (highly) asymmetric ODFs and error estimations using either only NN, NN + Tikhonov with $\tilde{g}_0(\theta,\phi) = 1$, NN + Tikhonov with $\tilde{g}_0(\theta,\phi) = 1$, or NN + QV. This material is available free of charge via the Internet at http://pubs.acs.org.

References and Notes

(1) Kashiwag, M.; Folkes, M. J.; Ward, I. M. *Polymer* **1971**, *12*, 697.
(2) Hentschel, R.; Schlitter, J.; Sillescu, H.; Spiess, H. W. *J. Chem. Phys.* **1978**, *68*, 56.
(3) Hentschel, R.; Sillescu, H.; Spiess, H. W. *Polymer* **1981**, *22*, 1516.
(4) Pick, M.; Lovell, R.; Windle, A. H. *Polymer* **1980**, *21*, 1017.
(5) Mitchell, G. R.; Windle, A. H. *Polymer* **1983**, *24*, 285.
(6) Mitchell, G. R.; Pick, M.; Windle, A. H. *Polym. Commun.* **1983**, *24*, 16.
(7) Mitchell, G. R.; Brown, D. J.; Windle, A. H. *Polymer* **1985**, *26*, 1755.
(8) Inoue, T.; Matsui, H.; Murakami, S.; Kohjiya, S.; Osaki, K. *Polymer* **1997**, *38*, 1215.
(9) Ward, I. M. *Structure and properties of oriented polymers*; Chapman and Hall: London, 1997.
(10) Sotta, P. *Macromolecules* **1998**, *31*, 3872.
(11) Ries, M. E.; Brereton, M. G.; Klein, P. G.; Ward, I. M.; Ekanayake, P.; Menge, H.; Schneider, R. *Macromolecules* **1999**, *32*, 4961.
(12) Utz, M.; Atallah, A. S.; Robyr, P.; Widmann, A. H.; Ernst, R. R.; Suter, U. W. *Macromolecules* **1999**, *32*, 6191.
(13) Utz, M.; Robyr, P.; Suter, U. W. *Macromolecules* **2000**, *33*, 6808.
(14) van Beek, J. D.; Meier, B. H.; Schäfer, H. *J. Magn. Reson.* **2003**, *162*, 141.
(15) Barakat, R.; Newsam, G. *Radio Sci.* **1984**, *19*, 1041.
(16) Craig, I. J. D.; Brown, J. C. *Inverse problems in Astronomy*; Adam Hilger: Bristol, U.K., 1986.
(17) Menke, W. *Geophysical Data analysis: Discrete Inverse Theory*; Academic Press: San Diego, CA, 1989.
(18) Hansen, P. C. *Rank-Deficient and Discrete Ill-Posed Problems: Numerical Aspects of Linear Inversion*; Monographs on Mathematical Modeling and Computation 4; SIAM: Philadelphia, PA, 1997.
(19) Sternin, E.; Bloom, M.; Mackay, A. L. *J. Magn. Reson.* **1983**, *55*, 274.
(20) Whittall, K. P.; Sternin, E.; Bloom, M.; Mackay, A. L. *J. Magn. Reson.* **1989**, *84*, 64.
(21) Grabowski, D.; Honerkamp, J. *J. Chem. Phys.* **1992**, *96*, 2629.
(22) Schäfer, H.; Stannarius, R. *J. Magn. Reson. Ser. B* **1995**, *106*, 14.
(23) Schäfer, H.; Madler, B.; Volke, F. *J. Magn. Reson. Ser. A* **1995**, *116*, 145.
(24) Schäfer, H.; Bauch, H. *Phys. Lett. A* **1995**, *199*, 93.
(25) Schäfer, H.; Madler, B.; Sternin, E. *Biophys. J.* **1998**, *74*, 1007.
(26) Vogt, F. G.; Aurentz, D. J.; Mueller, K. T. *Mol. Phys.* **1998**, *95*, 907.
(27) Winterhalter, J.; Maier, D.; Grabowski, D. A.; Honerkamp, J.; Muller, S.; Schmidt, C. *J. Chem. Phys.* **1999**, *110*, 4035.
(28) Sternin, E.; Schäfer, H.; Polozov, I. V.; Gawrisch, K. *J. Magn. Reson.* **2001**, *149*, 110.
(29) Zwanziger, J. W. *Solid State Nucl. Magn. Reson.* **1994**, *3*, 219.
(30) Utz, M. *J. Chem. Phys.* **1998**, *109*, 6110.

(31) Angeli, F.; Charpentier, T.; Faucon, P.; Petit, J. C. *J. Phys. Chem. B* **1999**, *103*, 10356.
(32) van Beek, J. D.; Beaulieu, L.; Schäfer, H.; Demura, M.; Asakura, T.; Meier, B. H. *Nature (London)* **2000**, *405*, 1077.
(33) van Beek, J. D.; Hess, S.; Vollrath, F.; Meier, B. H. *Proc. Natl. Acad. Sci. U.S.A.* **2002**, *99*, 10266.
(34) Song, Y. Q.; Venkataramanan, L.; Hurlimann, M. D.; Flaum, M.; Frulla, P.; Straley, C. *J. Magn. Reson.* **2002**, *154*, 261.
(35) Henrichs, P. M. *Macromolecules* **1987**, *20*, 2099.
(36) Schmidt-Rohr, K.; Hehn, M.; Schaefer, D.; Spiess, H. W. *J. Chem. Phys.* **1992**, *97*, 2247.
(37) Chmelka, B. F.; Schmidt-Rohr, K.; Spiess, H. W. *Macromolecules* **1993**, *26*, 2282.
(38) Lewis, R. H.; Long, H. W.; Schmidt-Rohr, K.; Spiess, H. W. *J. Magn. Reson. Ser. A* **1995**, *115*, 26.
(39) Wendlandt, M.; Tervoort, T. A.; Van Beek, J. D.; Suter, U. W. **2005**, *submitted for publication.*
(40) Ward, I. M. *Mechanical properties of solid poylmers*; John Wiley and Sons Ltd: Chichester, U.K., 1993.
(41) Tervoort, T. A.; Klompen, E. T. J.; Govaert, L. E. *J. Rheol.* **1996**, *40*, 779.
(42) Wendlandt, M. Finite Deformation of Polymeric Glasses: Continuum Modeling and Molecular Orientation, Thesis No. 15077, ETH Zurich, Zurich, Switzerland, 2003.
(43) Larson, R. G. *Constitutive equations for polymer melts and solutions*; Butterworths series in chemical engineering; Butterworths: Boston, MA, 1988.
(44) Baker, C. T. H.; Wright, K.; Fox, L.; Mayers, D. F. *Comput. J.* **1964**, *7*, 141.
(45) Hadamard, J. *Lectures on the Cauchy Problem in Linear Partial Differential Equations*; Yale University Press: New Haven, CT, 1923.
(46) Hansen, P. C. *Rank-deficient and discrete ill-posed problems*; Society for Industrial and applied methematics: Philadelphia, PA, 1998.
(47) Tikhonov, A. N.; Arsenin, V. Y. *Solutions of ill-posed problems*; John Wiley and Sons: New York, 1977.
(48) Engl, H. W.; Hanke, M.; Neubauer, A. *Regularization of Inverse Problems*; Kluwer Academic Publishers: Dordrecht, The Netherlands, 1996.
(49) Ivanov, V. K.; Vasin, V. V.; Tanana, V. P. *Theory of Linear Ill-Posed Problems and its Applications*; VSP: Utrecht, The Netherlands, 2002.
(50) Phillips, D. L. *J. ACM* **1962**, *9*, 84.
(51) Poggio, T.; Torre, V.; Koch, C. *Nature (London)* **1985**, *317*, 314.
(52) Grimson, W. E. L. *Philos. Trans. R. Soc. London, Ser. B−Biol. Sci.* **1982**, *298*, 395.
(53) Weese, J. *Comput. Phys. Commun.* **1992**, *69*, 99.
(54) Sundarar.Pr,; Flory, P. J. *J. Am. Chem. Soc.* **1974**, *96*, 5025.
(55) Lovell, R.; Windle, A. H. *Polymer* **1981**, *22*, 175.
(56) Schmidt, C.; Kuhn, K. J.; Spiess, H. W. *Prog. Colloid Polym. Sci.* **1985**, *71*, 71.
(57) Schmidt, C.; Blümich, B.; Wefing, S.; Kaufmann, S.; Spiess, H. W. *Ber. Bunsen-Ges. Phys. Chem. Chem. Phys.* **1987**, *91*, 1141.
(58) Long, G.; Grandjean, F. *The time domain in surface and structural dynamics*; Kluwer academic Publishers: Dordrecht, The Netherlands, 1988.
(59) Davis, J. H.; Jeffrey, K. R.; Bloom, M.; Valic, M. I.; Higgs, T. P. *Chem. Phys. Lett.* **1976**, *42*, 390.
(60) Brink, D. M.; Satchler, G. R. *Angular Momentum*, 2nd ed.; Clarendon Press: Oxford, U.K., 1968.
(61) Smith, S. A.; Levante, T. O.; Meier, B. H.; Ernst, R. R. *J. Magn. Reson. Ser. A* **1994**, *106*, 75.
(62) Fletcher, R. *Practical Methods of Optimization*; John Wiley and Sons: 1980.
(63) Wigner, E. *Gruppentheorie und ihre Anwendung auf die Quantenmechanik der Atomspektren*; Vieweg: Braunschweig, Germany, 1931.
(64) McBrierty, V. J. *J. Chem. Phys.* **1974**, *61*, 872.
(65) Roe, R. J. *J. Appl. Phys.* **1965**, *36*, 2024.
(66) Kratky, O. *Kolloid, Z.* **1933**, *64*, 213.
(67) Kuhn, W.; Grün, F. *Kolloid, Z.* **1942**, *101*, 248.
(68) Supporting Information is available free of charge. See paragraph at the end of the paper for more details.

MA0512105